Chemical Geology 525 (2019) 400–413

Contents lists available at ScienceDirect

Chemical Geology

journal homepage: www.elsevier.com/locate/chemgeo

Package fluids. Part 5: The NaCl-H_2O system in fluid inclusion research and applications of the software *AqSo_NaCl* (Bakker, 2018)

Ronald J. Bakker

Department of Applied Geosciences and Geophysics, Montanuniversity Leoben, Peter-Tunner-Str. 5, 8700 Leoben, Austria

ARTICLE INFO

Editor: Donald Dingwell

Keywords:
H_2O-NaCl
Fluid immiscibility
Fluid inclusions
Isochore
Microthermometry
Phase diagrams

ABSTRACT

The software *AqSo_NaCl* (Bakker, 2018) can be used to characterize the properties of phases that may exist in the binary H_2O-NaCl system up to 1000 °C and 500 MPa. The model replaces all available correlation equations and other equation of state that are restricted to narrow temperature, pressure, and composition intervals. Liquid-vapour, liquid-solid, and vapour-solid immiscibility fields emerge with increasing salinity at relative high temperatures, and already occur at mass fractions of a few µg per gram. The liquid-vapour immiscibility is split in two fractions in solutions between x(NaCl) = $2{\cdot}10^{-5}$ and 0.00025, at salinities that cannot be detected by microthermometry. Properties such as density, molar volume, composition, and volume fraction of liquid, vapour, and solid phases in fluid inclusions can be calculated in heating and freezing experiments. Isochores can be calculated within the homogeneous fluid field, within immiscibility fields, and along the *SLV* (solid-liquid-vapour) curve. Iso-T_h lines are obtained by modifying the total volume of fluid inclusion with the volumetric properties of quartz. Bulk properties of fluid inclusions can be directly calculated from microthermometric data.

1. Introduction

The H_2O-NaCl fluid system is characterized in numerous geochemical studies and is of major importance to the interpretation of fluid inclusions (e.g. Roedder, 1984). The thermodynamic properties of the entire composition range, i.e. from pure H_2O to pure NaCl, is described in the publication of Driesner and Heinrich (2007) and Driesner (2007). They provide an empirical equation of state that uses the unified Helmholtz energy function of pure H_2O (Haar et al., 1984) as a description of the pure end-member H_2O. Subsequently, the parameters in this function are corrected with purely empirical equations to take into account a specific salinity. Bakker (2018) developed the software *AqSo_NaCl* to facilitate the use of this equation of state, and added the possibility to calculated isochores of fluid inclusions, which may be corrected for the volumetric properties of the quartz host (e.g. Hosieni et al., 1985). The software offers the possibility to construct numerous phase diagrams with the parameters *p-T-V-x* (pressure, temperature, volume, and mole fraction). A small part of this collection is regularly used in fluid inclusion studies to interpret microthermometric data, for example as illustrated in Shepherd et al. (1985), but they are usually restricted to a very limited range of temperatures, pressures and mole fractions.

The major objective of the present work is to present the application possibilities of the software *AqSo_NaCl* (Bakker, 2018), to visualize the development of immiscibility regions in the binary H_2O-NaCl system, and to specify the development of phases within fluid inclusions in heating and freezing experiments. The differences between isochores and *iso-T_h* lines (e.g. Zhang and Frantz, 1987) are illustrated with several examples, and the accuracy of the model is compared to experimental data and a variety of correlation equations and equations of state.

2. Development of the bubble-point, dew-point and sublimation curve up to microthermometry detectable salinities

The phase diagram of pure water (e.g. Haar et al., 1984) is occasionally used in fluid inclusion research to characterize density, isochores and trapping conditions. Invariant points such as the triple point and the critical point, are connected with univariant lines and divariant fields in various two dimensional phase diagrams composed by the parameters temperature (T), pressure (p), molar volume (V_m) (e.g. Diamond, 2003a). Immiscibility of phases such as liquid, vapour and solid, occurs at the liquid-vapour curve, liquid-solid curve, and solid-vapour curve at very limited temperature-pressure conditions that do not usually occur in sediments and rock. The liquid-vapour curve combines the bubble-point curve (i.e. homogenization in to the liquid phase, $LV \rightarrow L$) and dew-point curve (i.e. homogenization in to the vapour phase, $LV \rightarrow V$) in a single line in a pT diagram.

E-mail address: bakker@unileoben.ac.at.

https://doi.org/10.1016/j.chemgeo.2019.07.041
Received 21 December 2018; Accepted 31 July 2019
Available online 05 August 2019

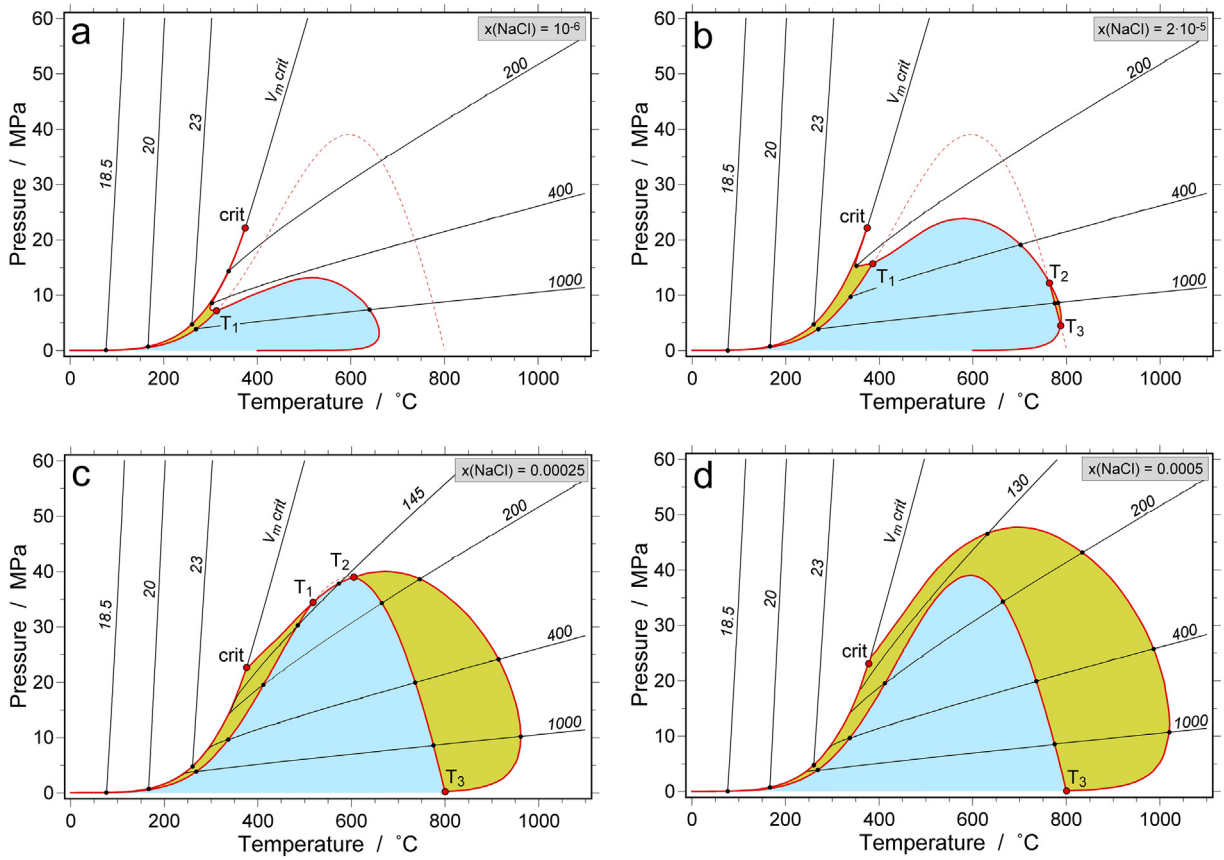

Fig. 1. Temperature-pressure diagrams of dilute NaCl-bearing aqueous solutions: **a**. x(NaCl) = 10^{-6}; **b**. x(NaCl) = $2{\cdot}10^{-5}$; **c**. x(NaCl) = 0.00025; **d**. x(NaCl) = 0.0005. The thin solid black lines are isochores, indicated with a molar volume value (cm^3/mol). The critical isochore (**V_m crit**) divides the homogeneous fluid field in a liquid-like and vapour-like fluid field. The dashed red line is a projection of the *SLV* curve. The solid red lines illustrate the limits of the immiscibility fields. The light-blue field represents solid-vapour immiscibility, and the yellow-green field liquid-vapour immiscibility. **Crit.** = the critical point of a specific fluid composition. **T_1**, **T_2** and **T_3** are triple points of liquid-vapour-halite coexistence at the *SLV* curve, i.e. the intersection of three fields (*SV*, *LV*, and homogeneous fluid field). See text for further details. (For interpretation of the references to colour in this figure legend, the reader is referred to the web version of this article.)

Addition of small amounts of NaCl, for example a few μg/g, to a pure H_2O system has a large effect on the conditions of fluid immiscibility (Fig. 1). Natural fluids in rock are not composed of pure H_2O, but are always aqueous solutions that contain certain amounts of dissolved ions. Very low concentrations in the range of μg/g to mg/g are detected by Laser-ablation ICP-MS analyses in most natural fluid inclusions (e.g. Pettke et al., 2012; Leisen et al., 2012), which illustrates that these immiscibility fields must exist in most natural systems. For example, the solubility of minerals such as quartz and calcite in aqueous solutions may reach values in the range of 0.01 to 0.01 m as a function of temperature and pressure (e.g. Newton and Manning, 2000; Duan and Li, 2008), and it is expected that these ionic concentrations affect the immiscibility in H_2O-rich fluids in a similar way.

Fig. 1a illustrates modifications of a pure H_2O system by adding 1 μmol NaCl to 1 mol of H_2O, corresponding to a molality of $5.6{\cdot}10^{-5}$. This composition develops a huge vapour-solid immiscibility field up to 660.5 °C and 13.19 MPa enclosed in a sublimation-point curve. The bubble-point curve is not significantly affected by this small amount of salt, whereas the dew-point curve is restricted to the temperature range 298.9 to 374.0 °C. These two lines define the limits of the liquid-vapour immiscibility field. The critical point cannot be distinguished from a pure H_2O system, because it is shifted with only +0.012 °C and + 0.003 MPa. Isochore intersections with immiscibility fields are the homogenization conditions within fluid inclusions. Homogenization in to the liquid phase (bubble-point curve) cannot be distinguished from a pure H_2O system, whereas homogenization in the vapour phase (dew-point curve) cannot occur at temperatures below 298.9 °C, unlike a pure H_2O system. In the range 298.9 to 313.0 °C (T_1 in Fig. 1a), the dew point curve has two solutions at one specific temperature. Consequently, this homogenization temperature cannot be used directly to calculate a unique bulk density. Similarly, a temperature measurement of sublimation in the range 313.0 to 660.5 °C does not result in a unique solution of density and pressure. At the same temperature, relative high densities sublime at higher pressure, whereas relative low densities sublime at lower pressures. Volume fractions of the solid phase at room temperature provide the additional information to obtain a unique solution.

The vapour-solid and liquid-vapour immiscibility fields increase in size at higher salinities (Fig. 1b). A fluid with x(NaCl) = $2.0{\cdot}10^{-5}$ develops a second liquid-vapour immiscibility field at high temperatures (Fig. 2a), between 763.7 and 787.8 °C (T_2 and T_3 in Fig. 1b), due to the intersection of the vapour-solid immiscibility field with the *SLV* curve. This immiscibility field is limited by homogenizations only in to the vapour field (dew-point curve). High molar volume isochores (i.e. low-density) may intersect both liquid-vapour immiscibility fields, which is characterized by the appearance and disappearance of small amounts of a liquid phase and halite crystal (e.g. the 1000 cm^3/mol isochore in Fig. 1b). The critical point of this fluid composition is 374.2 °C and 22.11 MPa that cannot be distinguished from a pure H_2O system with microthermometry, according to the precision and accuracy of this method.

The vapour-solid immiscibility field has reached approximately its maximum size at x(NaCl) = 0.00025, with the upper pressure limit defined by the *SLV* curve (Fig. 1c). The upper temperature limit of the

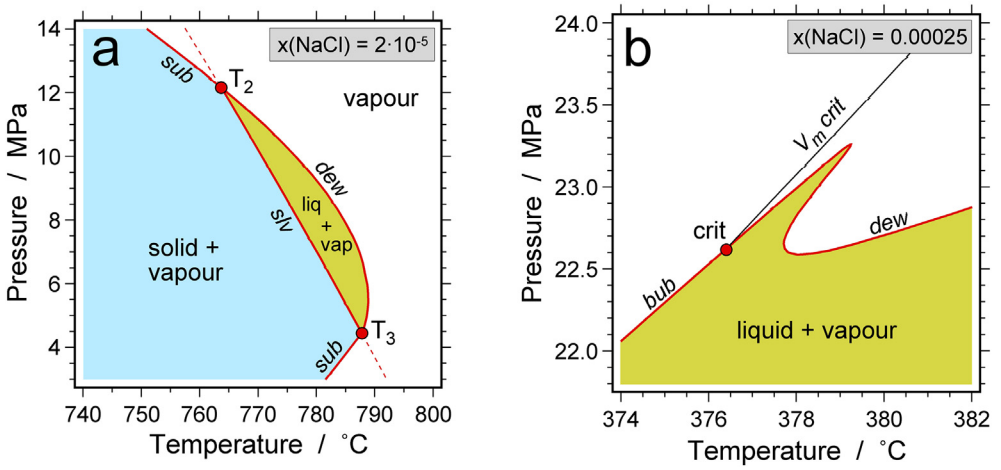

Fig. 2. Temperature-pressure diagram with the additional liquid-vapour immiscibility field for x(NaCl) = $2{\cdot}10^{-5}$ (**a**) and the doubly bended dew-point curve near the critical point for x(NaCl) = 0.00025 (**b**). *bub* = bubble-point curve, *dew* = dew-point curve, *sub* = sublimation-point curve. Definitions of other points, lines and fields see Fig. 1. See text for further details.

second liquid-vapour immiscibility field has drastically expanded up to 962 °C within this relative small compositional range. At slightly higher salinities, the two separate liquid-vapour immiscibility fields are united, e.g. at x(NaCl) = 0.0005 (Fig. 1d). The critical point of the x (NaCl) = 0.00025 aqueous solution is shifted to 376.4 °C and 22.62 MPa. Close examination of temperature-pressure conditions near the critical point reveal a complex morphology of the dew-point curve (Fig. 2b). The dew point curve has three intersections at a selected temperature between 377.7 and 379.3 °C due to its doubly bended shape.

The phase diagram illustrated in Fig. 1d represents a fluid system with x(NaCl) = 0.0005, that corresponds to a measureable effect in microthermometrical experiments. However, consideration of the accuracy of these temperature measurements the smallest amount of detectable salt correspond to a freezing-point depression of approximately −0.2 °C. This temperature reflects a salinity of x(NaCl) = 0.0011, 0.35 eq. mass% NaCl, and 0.06 molality NaCl. At x(NaCl) = 0.0005, the *p-T* phase diagram already illustrates a large liquid-vapour immiscibility field up to 1021 °C and 47.69 MPa (Fig. 1d), whereas the vapour-solid immiscibility field has reached it maximum size at *T-p* conditions below the *SLV*-curve. A special novelty of this phase diagram is that homogenization in to the vapour phase (dew-point) always occurs at higher temperatures than homogenization in to the liquid phase (bubble point). This may elucidate the difficulty with which vapour-rich fluid inclusions are analyzed with microthermometry, in addition of optical limitations.

The type of phase diagrams illustrated in Fig. 1 is suggested to represent natural fluid systems that are assumed to be nearly pure H_2O. The phase separation at high temperature and relative low pressures may have important consequence for fluid-rock interactions at realistic geological conditions, such as described in contact metamorphism and shallow magmatism. The formation of a large vapour-solid immiscibility field may cause the crystallization of salt crystals out of a hot vapour-like aqueous fluid at these conditions.

3. Immiscibility at higher salinities

The immiscibilities of liquid, vapour and solid (halite) phases in NaCl-bearing aqueous solutions at salinities higher than x(NaCl) = 0.01 (3.17 mass% NaCl) is mainly defined by a large temperature-pressure field of liquid-vapour and liquid-solid unmixing (Fig. 3). The upper temperature limit of liquid-vapour immiscibility is unknown due to the lack of experimental data at extreme high temperatures. The maximum size of this field is obtained at about x(NaCl) = 0.15 (36.4 mass%) (Fig. 3c). The vapour-solid immiscibility field remains anchored below the *SLV*-curve with a maximum temperature of about 800 °C (i.e. the triple point of pure NaCl) and a maximum pressure of about 39 MPa. The liquid-solid (halite) immiscibility field enters this diagram at low temperatures and at salinities exceeding x(NaCl) = 0.1 (Fig. 3b). This field is rapidly expanding with increasing salinities towards higher temperatures, at the cost of conditions of a homogeneous liquid-like fluid mixture (c.f. Fig. 3b and Fig. 3d). The upper pressure limit of liquid-solid (halite) immiscibility is unknown due to the lack of experimental data exceeding 500 MPa. At x(NaCl) = 0.5 (76 mass%) the phase assemblages in a temperature-pressure diagram are mainly defined by immiscibility fields (Fig. 3d). Consequently, isochores of homogeneous NaCl-H_2O fluid mixtures are restricted to only a small range at extreme high temperature-pressure conditions. The critical point reaches the limits of the model already at x(NaCl) = 0.1345 (33.5 mass%), at 1000 °C and 216 MPa. Consequently, only the bubble point curve ($LV \rightarrow L$) and the dissolution curve ($SL \rightarrow L$) define the limits of the homogeneous fluid field at higher salinities.

The dew-point curve always occurs at higher temperature-pressure conditions than the bubble-point curve (e.g. Fig. 3a and b), similar to Fig. 1d. At temperatures exceeding 800 °C, an additional low-pressure branch of the dew-point curve result occasionally in a double intersection at a selected temperature. For example, a fluid composition x (NaCl) = 0.01 (3.17 mass%) and a hypothetical homogenization temperature of 850 °C ($LV \rightarrow V$) correspond to a density of 0.2721 g/cm^3 (67.68 cm^3/mol) in the high-pressure branch at 118.1 MPa, and to a density of 0.00003 g/cm^3 (688,269 cm^3/mol) in the low pressure branch at 0.013 MPa. The high density fluid inclusions contain 26.6 vol % liquid phase at room temperature, whereas the low density fluid inclusions contain only $3.4{\cdot}10^{-18}$ vol% liquid. It is unlikely that the lower branch homogenization can be observed in fluid inclusions because the volume fraction of the liquid phase at room temperatures is extremely low. These inclusions appear as all-vapour fluid inclusions, although a minor amount of saline aqueous liquid with x (NaCl) = 0.025 (7.68 mass%) is wetting the inclusion walls.

The T_4 temperature (Fig. 3b, c, and d) is often mistaken for a direct measure of the bulk salinity (e.g. Sterner et al., 1988), corresponding to the dissolution temperature of a halite crystal in a fluid inclusion in the presence of a vapour phase. However, homogenization at T_4 corresponds to the phase transition $SLV \rightarrow L$, which is the lowest possible dissolution temperature in the presence of a vapour phase for one specific bulk salinity (e.g. Bakker, 2012). A large range of dissolution temperatures is possible for a constant bulk salinity depending on the bulk density of the inclusion, i.e. the relative size of the vapour bubble at room temperatures. This is visualized in Fig. 3 with the intersection of various isochors within the *LV* immiscibility field and the *SLV* curve at temperatures exceeding T_4.

Isochores within immiscibility fields (*SL*, *LV*, and *SV*) are composed of two coexisting phases with specific individual density, composition and volume fraction within a closed system, that sums up to the

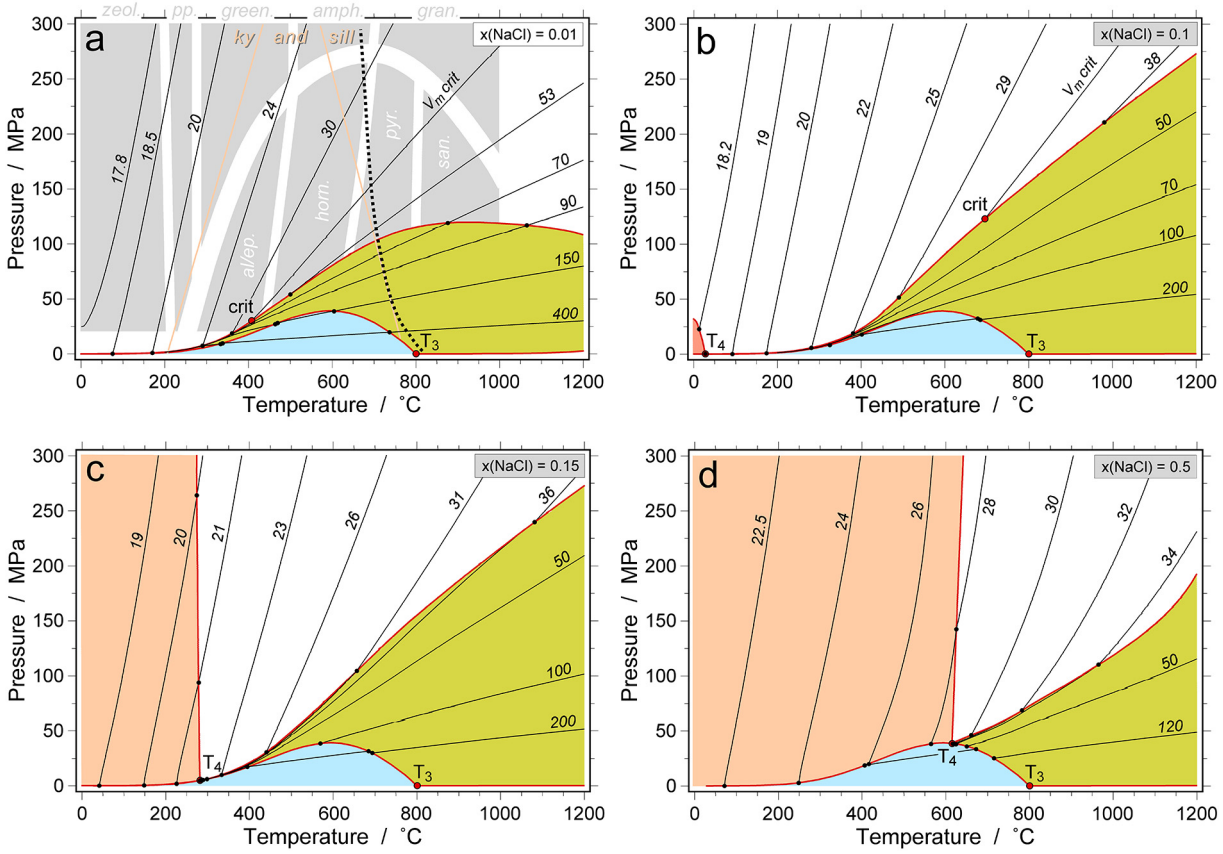

Fig. 3. Temperature-pressure diagrams of saline NaCl-bearing aqueous solutions: **a**. x(NaCl) = 0.01; **b**. x(NaCl) = 0.1; **c**. x(NaCl) = 0.15; **d**. x(NaCl) = 0.5. Explanation symbols see Fig. 1. Additional symbols: the pink field represents solid-liquid immiscibility, $\mathbf{T_4}$ is a triple point of liquid-vapour-halite coexistence at the *SLV* curve at relative low temperatures. The grey shaded areas in (**a**) illustrate metamorphic facies: zeolite facies (*zeol.*), prehnite-pumpellyite facies (*pp.*), greenschist facies (*green.*), amphibolite facies (*amph.*), granulite facies (*gran.*), albite-epidote hornfels facies (*al/ep.*), hornblende hornfels facies (*horn.*), pyroxene hornfels facies (*pyr.*) and sanidine hornfels facies (*san.*). The Al_2SiO_5 polymorphs stability fields (andalusite, kyanite, and sillimanite) are defined according to Holdaway and Mukhopadhyay (1993). (For interpretation of the references to colour in this figure legend, the reader is referred to the web version of this article.)

selected bulk properties. Low density isochores reveal a clear break in slope upon entering from the *LV* field into the *SV* field (e.g. Fig. 3d). For example, the *SLV* curve is reached at 715.5 °C after cooling along the 120 cm^3/mol isochore for a x(NaCl) = 0.5 fluid mixture in the *LV* field. Upon further cooling, the isochore follows the *SLV* curve down to 672.7 °C, before it is entering within the SV field, whereas the pressure increases from 25.05 to 33.20 MPa. The isochores within the *LV* immiscibility field apparently intersect the bubble- point curve at lower temperatures. For example, the 70 cm^3/mol isochore in Fig. 3a has a homogenization temperature of 876.6 °C (dew point curve, $LV \rightarrow V$). At lower temperatures, this sub-isochore approaches the bubble-point curve, but it does not intersect this curve.

The association of the H_2O-NaCl system with metamorphic facies (e.g. Winter, 2014; Bucher and Grapes, 2010) and magmatic systems is illustrated in Fig. 3a. Defined by the bulk salinity of the fluid system *LV* immiscibility and *SV* immiscibility may occur in the low-pressure facies (contact metamorphism), whereas *SL* immiscibility may occur in medium and high pressure facies. In addition, high temperature granulite facies at relative low pressure may locally include *LV* immiscibility. Greenschist, amphibolite, and granulite facies metamorphic rock may contain a homogeneous H_2O-NaCl-rich liquid-like fluid that correspond to bubble-point homogenizations in fluid inclusions. At high salinities, i.e. x(NaCl) > 0.15, halite crystals may precipitate from this brine when the metamorphic conditions are located in the *SL* immiscibility field. Granulite-facies rock may also reveal H_2O-NaCl-rich fluid inclusions, i.e. for x(NaCl) < 0.1, that homogenize at the dew-point curve at near-critical conditions. Similar fluid properties can be obtained in contact metamorphism (albite-epidote hornfels, hornblende hornfels, pyroxene hornfels, and sanidine hornfels facies) but terrains with very high geothermal gradients are located within the *LV* and *SV* immiscibility fields. The stability field of kyanite corresponds to relative high density H_2O-NaCl fluids (Fig. 3a) that may reveal *SL* immiscibility at higher salinities. Andalusite is restricted to homogeneous liquid-like fluid mixtures, in addition to near-critical vapour-like fluid mixtures at salinities x(NaCl) < 0.1. The variability of fluid mixture properties in the sillimanite field is defined by pressure conditions in the rock. At relative low pressure sillimanite coexists with immiscible liquid and vapour phases, at intermediate pressures with a homogeneous vapour-like fluid, and at high pressures with a homogeneous liquid-like fluid. At very high salinities (Fig. 3d), the fluid properties within the sillimanite stability field are defined by *LV* immiscibility at relative low pressures, and homogeneous liquid-like fluid mixture at higher pressures. The water-saturated granite solidus nearly coincide with the limits of the sillimanite stability field at relative low pressures (Fig. 3a). Consequently, similar fluid properties are predicted in a magmatic system.

4. Bulk density and composition calculations

Two intensive thermodynamic parameters have to be measured or determined to characterize the bulk properties of a binary fluid system within fluid inclusions, which is a direct application of the Gibbs phase-rule (e.g. Diamond, 2003a). It should be noted that the low solubility of the host mineral is neglected because it does not affect significantly the H_2O-NaCl fluid properties in fluid inclusions. Microthermometry and optical microscopy offer a variety of parameters that can be used for

this modelling: 1. dissolution temperature T_m (*SLV* → *LV* and *SL* → *L*); 2. homogenization temperature T_h (*LV* → *L*, *LV* → *V*, and *SLV* → *SL*); and 3. volume fraction estimates. In literature, dissolution often refers to completely dissolving a solid phase, such as ice, hydrohalite, or halite in liquid and/or vapour, and homogenization refers to dissolving the vapour in its coexisting liquid phase, or vice versa, in the presence or absence of a solid phase. Both processes refer to a reduction of the number of daughter phases upon heating in a closed system.

Mathematical definitions of the bubble-point curve and the dew-point curve are used to calculate density (molar volume) from homogenization temperatures. Highly accurate equations are available for pure-fluid systems such as pure H_2O (e.g. Haar et al., 1984), and pure CO_2 (e.g. Span and Wagner, 1996). This accuracy is often missing for binary mixtures, where dew-point curves and bubble-point curves do not coincide at the same temperatures and pressures. Mathematical definitions of *SLV* (where *S* = halite), ice dissolution curve, and hydrohalite dissolution curve can be used to calculate salinity. Abundant purely empirical equations are available in literature that describe these modifications in phase assemblages within only a limited range of conditions. Driesner and Heinrich (2007) and Driesner (2007) condense all these equations in to one complex model that includes a nearly complete description of the H_2O-NaCl system up to 1000 °C and 500 MPa, and that was incorporated in the software *AqSo_NaCl* (see further details in Bakker, 2018). Volume fraction of the vapour phase within fluid inclusions at room temperatures can be estimated with the method of Bakker and Diamond (2006).

The program *AqSo_NaCl* contains two windows to calculate bulk fluid properties from the previously described parameters: 1. *"Liquid and Vapour Coexistence"* (bubble-point and dew-point); and 2. "*Microthermometry*", that can be selected in the start menu. The latter is a direct application to fluid inclusions studies. The input parameters of the first window are temperature or pressure of total homogenization, in addition to composition in the binary H_2O-NaCl system. The complexity of dew-point-curve (*LV* → *V*) may result in multiple solutions at different pressures and one selected temperature (see Figs. 1, 2, and 3). Selection of one of these solutions results in the calculation of corresponding fluid properties, such as composition (mole fraction, mass%), molar volume, density, enthalpy, and heat capacity of the individual vapour, liquid and solid phases (see further details in Bakker, 2018). The software offers the possibility to calculate temperature and pressure limits of a specific *LV* immiscibility field of a specific composition. For example, at 700 °C and 50 MPa a liquid phase of 77.58 mass% NaCl and 30.81 cm^3/mol coexist with a vapour phase of 0.19 mass% NaCl and 138.44 cm^3/mol. However, at 200 MPa and the same temperature, conditions are well within the homogeneous fluid field.

The window "Microthermometry" in the program *AqSo_NaCl* is specially designed to handle directly dissolution temperatures, homogenization temperatures, and volume fraction of the liquid and vapour phase to calculate the bulk fluid properties (density and composition) of fluid inclusions. Dissolution refers to the same process as homogenization in the sense of reducing the number of phases in a specific phase assemblage within fluid inclusions. Therefore, the corresponding temperatures are described as the reduction of three-to-two and two-to-one phases. The former describes three different processes: 1. *SLV* → *LV*, 2. *SLV* → *SL*, and 3. *SLV* → *SV*, where the solid phase is ice, hydrohalite, or halite. The latter describes four different processes: 1. *LV* → *L*, 2. *LV* → *V*, 3. *SL* → *L*, and 4. *SV* → *V*, where the solid phase is halite. This final heating experiment results in the total homogenization into a "liquid-like" phase (high density) or "vapour-like" phase (low density). The term "liquid-like" and "vapour-like" is used to specify its mode of homogenization. The stability temperature and pressure conditions of a liquid-like and a vapour-like homogeneous fluid are separated by the isochore of the critical density. The T_m and T_h values of one fluid inclusion cannot vary independently (Bakker, 2012). Moreover, the mode of total homogenization, either in to the liquid or vapour phase must be consistent with the detected dissolution temperature. The software offers the possibility to calculate those limits by a number of hypothetical settings based on the selected T_m value and a range of volume fraction of the liquid phase. This procedure determines critical point temperatures that defines the end points of the dew-point curve and bubble-point curve. In absence of a T_h measurement due to temperature limits of used stage, optical difficulties, or decrepitation at higher temperature, the volume fraction of the liquid phase at room temperatures can be introduced to calculate the bulk fluid properties of inclusions (see further details in Bakker, 2018).

T_m and T_h values may be separated by a large temperature interval. The molar volume of the quartz host may be significantly modified during a heating experiment to measure both temperatures. The calculations may include a correction to take into account the change in the total volume of a fluid inclusion using the quartz equation of state from Hosieni et al. (1985). For example, the ice dissolution temperature in a fluid inclusion is −20 °C (*SLV* → *LV*) and the homogenization temperature is 600 °C (*LV* → *L*). The bulk composition and density of this inclusion are 22.38 mass% NaCl and 0.6367 g/cm^3, respectively, without correction of the quartz volume. These values are modified to 22.38 mass% NaCl and 0.6651 g/cm^3 taking into account the modification of the quartz volume. The volume fraction of liquid at room temperature is modified from 54.54% to 56.98%. The relative change in bulk density and volume fraction is +4.4%.

5. Isochores and sub-isochores

The software *AqSo_NaCl* offers the possibility to construct an isochore within the homogeneous fluid field, within coexisting two-phase fields (*LV*, *SL*, and *SV*) and along the three-phase curve (*SLV*) within temperature-pressure diagrams (Figs. 1 and 3). The isochores within the two-phase fields and the three-phase curve (further indicated with "*sub-isochore*") are not isochores in the sense of one homogeneous fluid, but the combination of two or three phases with specific properties and volume fractions that sum up to a constant bulk density and composition. These restrictions can be directly applied to closed-system fluid inclusions at variable temperatures. The calculated isochores and sub-isochores with *AqSo_NaCl* describe the properties of each individual phase (composition, density, and volume fraction) within fluid inclusions during a heating and freezing experiment.

Fig. 4 illustrates an example of a heating experiment with a fluid inclusion of x(NaCl) = 0.1 (w = 26.495%) and bulk molar volume 29 cm^3/mol. At room temperature, this fluid inclusion may contain a very small halite crystal (0.04 vol%) that most probably is metastably absent, and that would have a dissolution temperature of 27.0 °C. In addition, this fluid inclusion contains 36.7 vol% vapour phase, and 63.3 vol% liquid phase. Heating from room temperature to the homogenization temperature (490.3 °C, LV → *L*) occurs along the sub-isochore in the presence of a liquid and vapour phase, that modify continuously in composition, density and volume fraction until the homogenization. The rate in pressure modification increases at higher temperatures (Fig. 4a). Around the homogenization temperature, the slope of the sub-isochore and the isochore do not significantly differ. Consequently, this specific example illustrate that the limits of the *LV* immiscibility field are difficult to estimate from an abrupt change in experimentally obtained slopes (c.f. Gehrig, 1980; Gehrig et al., 1986). The volumetric development of the vapour bubble of this fluid inclusion upon heating is illustrated in Fig. 4b. Similar to the pressure, the rate of volume fraction modification of the vapour bubble increases at higher temperatures. Consequently, during a heating experiment with a constant heating rate, the volume fraction modification increases rapidly, and the measurement of homogenization may be overestimated. An unexpected change in the salinity of the liquid phase along this sub-isochore is illustrated in Fig. 4c: the salinity increases upon heating and reaches a maximum value (approximately +3%) at about 420 °C. Mechanical mixing in an open system by adding a low salinity vapour to a high salinity liquid phase generally results in a decrease of the salinity

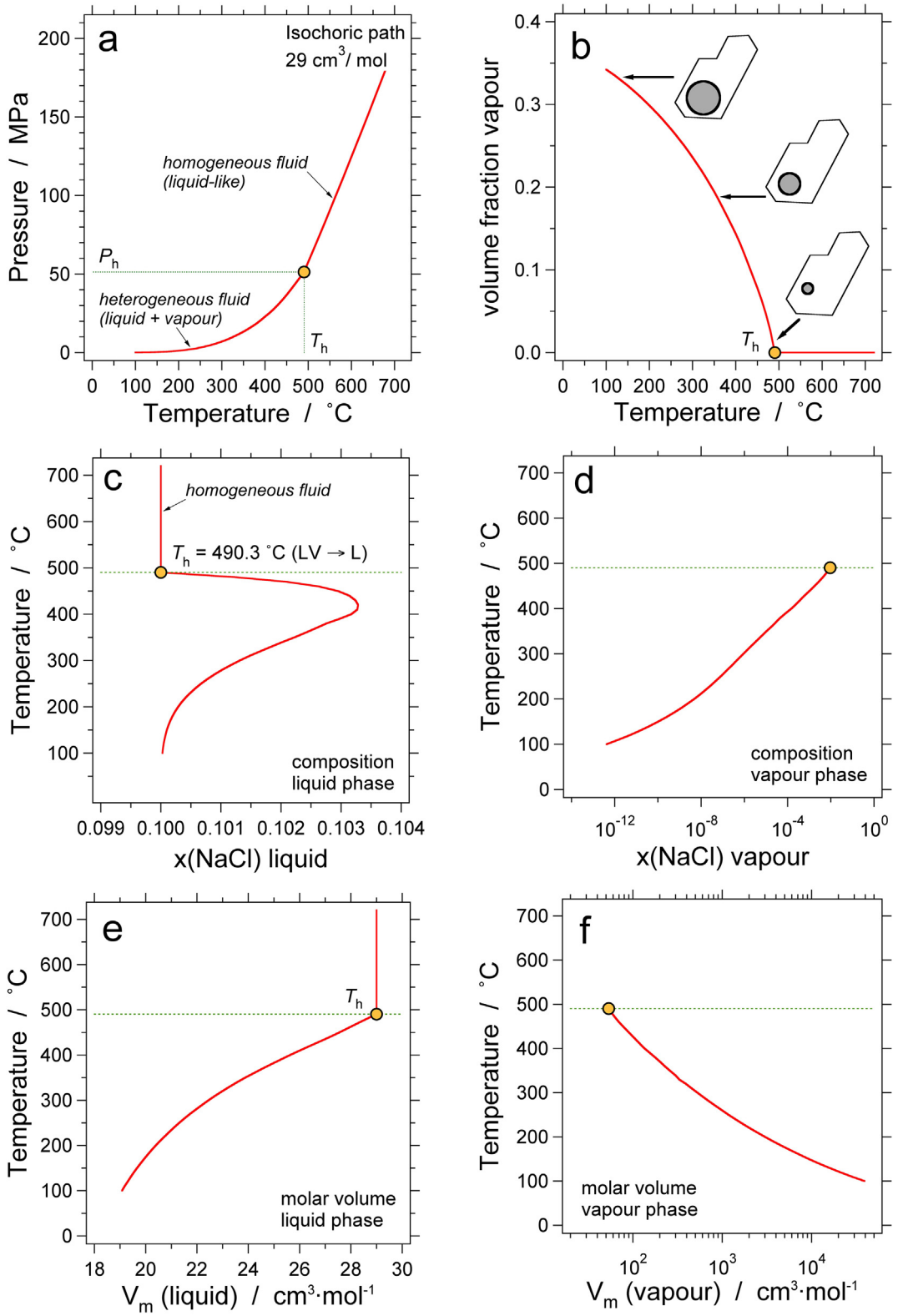

Fig. 4. Series of phase diagrams with the parameters temperature, pressure, molar volume and composition illustrating the properties of a fluid inclusion along the sub-isochore and isochore. See text for further detail.

of the liquid phase. However, within a closed system such as a fluid inclusion, the combination of modifications in composition, density and volume fraction of each phase results in the opposite effect. The salinity of the vapour phase is continuously increasing upon heating (Fig. 4d), until disappearance at homogenization. The molar volume of the liquid phase increases from 18.4 cm^3/mol at room temperature to 29 cm^3/mol at the homogenization temperature, whereas the vapour phase decreases from $1.8{\cdot}10^6$ cm^3/mol to 53.6 cm^3/mol (Fig. 4e and f). The complete set of values of the sub-isochore and isochore in Fig. 4 calculated with the software *AqSo_NaCl* are illustrated in Supplementary

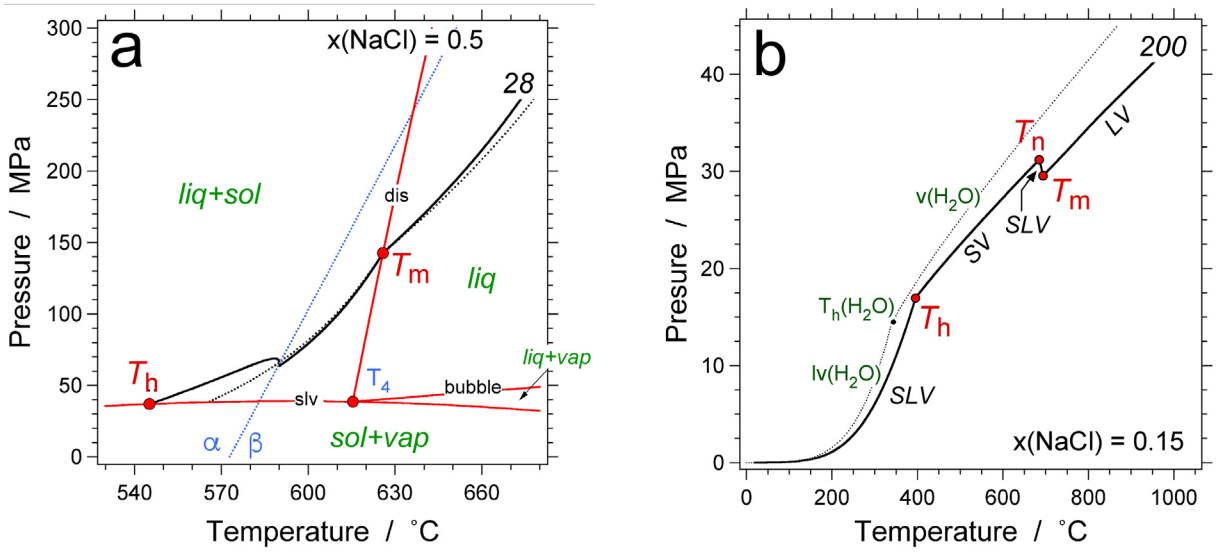

Fig. 5. Temperature-pressure phase diagrams with isochores and sub-isohores for the fluid systems: (**a**) x(NaCl) = 0.5 and 28 cm^3/mol. The solid black curve is the isochore corrected for quartz volume modifications. The dashed black curve is the uncorrected isochore. The blue dashed line is the α-β quartz transition, the fields are indicated with the corresponding phase assemblage in green. The red lines are the *SLV* curve, bubble-point curve (*bubble*) and dissolution curve (*dis)*; (**b**) x (NaCl) = 0.15 and 200 cm^3/mol. The dashed black curve is the sub-isochore and isochore of a pure H_2O system with the same molar volume. See text for further details. (For interpretation of the references to colour in this figure legend, the reader is referred to the web version of this article.)

data.

Isochores in a homogeneous fluid system have positive slopes in a temperature-pressure diagram. However, there are two exceptions to this general rule in closed systems: 1. nearly pure H_2O fluids have isochores with negative slope below 4 °C according to the special properties of water (e.g. Diamond, 2003a); and 2. the modification of the total volume of inclusions in quartz near the α-β transition exceeds the compressibility properties of the fluid resulting in a negative slope of isochores and sub-isochores. In addition, sub-isochores along the *SLV*-curve may also reveal a negative slope at temperatures above 594 °C. A hypothetical fluid inclusion with bulk properties 28 cm^3/mol and x(NaCl) = 0.5 (Fig. 5a) reveals a halite dissolution temperature of 625.8 °C (*SL* → *L*). The sub-isochore within the *SL* field crosscut the α-β transition of quartz at about 590 °C and 66.7 MPa. Due to compressibility differences the sub-isochore has a negative slope in the α-quartz stability field close to this transition. The homogenization at the *SLV* curve (*SLV* → *SL*) occurs at 545.2 °C, whereas fluid properties in the absence of quartz volume corrections result in a homogenization at 565.4 °C (see dashed sub-isochore curve in Fig. 5). Furthermore, the corrected isochore has a steeper slope than the uncorrected isochore in the homogeneous fluid field. A second hypothetical fluid inclusion with bulk properties 200 cm^3/mol and x(NaCl) = 0.15 is illustrated in Fig. 5b. This fluid example does not reach a total homogenization upon heating up to 1000 °C, consequently, only the sub-isochore can be calculated with the software *AqSo_NaCl*. At room temperatures, this inclusion contains the phase assemblage vapour, brine and halite with volume fractions 90.58%, 8.67% and 0.75%, respectively. The liquid and solid phase will be difficult to detect in most natural fluid inclusion due to optical limitations, however, flat-shaped inclusions may reveal a brine that wets the inclusion walls. The salinity of the liquid phase increases upon heating from x(NaCl) = 0.0996 to 0.2117 at the partial homogenization temperature *SLV* → *SV* (T_h in Fig. 5b). In the same temperature interval, the volume fraction of the halite crystal increases to 2.12%. At 685.0 °C, the liquid phase is nucleated again (T_n in Fig. 5b) and further heating results in a pressure drop in the system as the sub-isochore follows the *SLV* curve. Within a relative short temperature interval, the solid phase rapidly dissolve completely at 694.1 °C (T_m in Fig. 5b), whereas the liquid phase is a highly saline brine, i.e. x (NaCl) = 0.658 to 0.678, that occupies only 3.5 vol% of the fluid inclusion. Upon further heating, the volume fraction and the salinity of the liquid phase increase to 3.7 vol% and x(NaCl) = 0.772 (91.67 mass % NaCl). This example illustrates that a highly saline brine can be generated out of a hot medium to low salinity vapour phase. Moreover immiscibility of the fluid phase may increase upon heating this water-salt system, in contrast to an expected homogenization process. For comparison, the isochoric path of a pure H_2O fluid inclusion with the same molar volume is illustrated in Fig. 5b. It should be noted that the densities are significant different of these systems, c.f. 0.1204 g/cm^3 for x(NaCl) = 0.15 and 0.0901 g/cm^3 for pure H_2O. The isochore of the pure H_2O inclusion occurs at increasingly higher pressures than the isochore at x(NaCl) = 0.15 upon heating after total homogenization at 338.5 °C (*LV* → *V*). In microscopic research, these theoretical calculations illustrate an example of two fluid inclusions with different bulk properties that can be easily confused due to optical limitations on the visibility of phases with a low volume fraction within fluid inclusions. The complete set of calculated values of the sub-isochore and isochore in Fig. 5 are illustrated in Supplementary data.

6. "Iso-T_h" lines

The interpretation of microthermometrical analyses from fluid inclusions that are suspected to contain mainly H_2O and NaCl was based on the use of highly simplified fluid models also known as "correlation" equations, due to lack of comprehensive algorithms that describe *p-T-V-x* properties of liquids, vapours and solids of the H_2O-NaCl system over the complete range of conditions of interest. Experimental studies of synthetic fluid inclusions were used to develop simplified models that relate experimental trapping conditions to homogenization temperatures (e.g. Zhang and Frantz, 1987; Bodnar, 1995). These models were used to design the so-called "iso-T_h" lines, i.e. temperature-pressure conditions in the homogeneous fluid field that result in the same homogenization conditions, without any knowledge about density. These iso-T_h lines are per definition linear, and they are designed from a best-fit to at least two *T-p* data points (i.e. homogenization and experimental conditions). However, iso-T_h lines may be highly inaccurate at conditions between the two points or at extrapolated conditions.

The iso-T_h lines are equal to isochores if the total volume of the inclusions is constant, and the density of inclusions is not modified

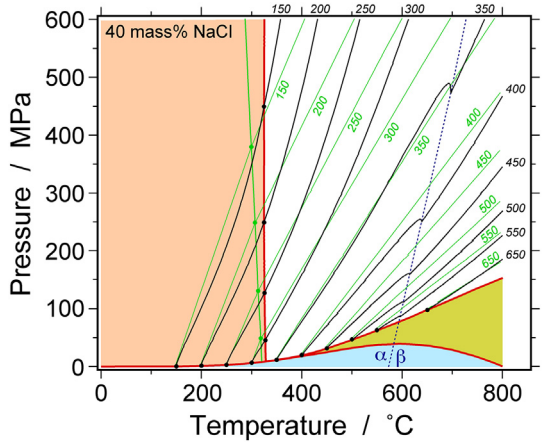

Fig. 6. Iso-T_h lines (green: Bodnar, 1994, 2003) and curves (black: Bakker, 2018) for fluid inclusions with a salinity of 40 mass% NaCl. The dark-blue dashed line is the α-β transition of quartz. Colouring of the fields according to Figs. 1 and 3. See text for further details. (For interpretation of the references to colour in this figure legend, the reader is referred to the web version of this article.)

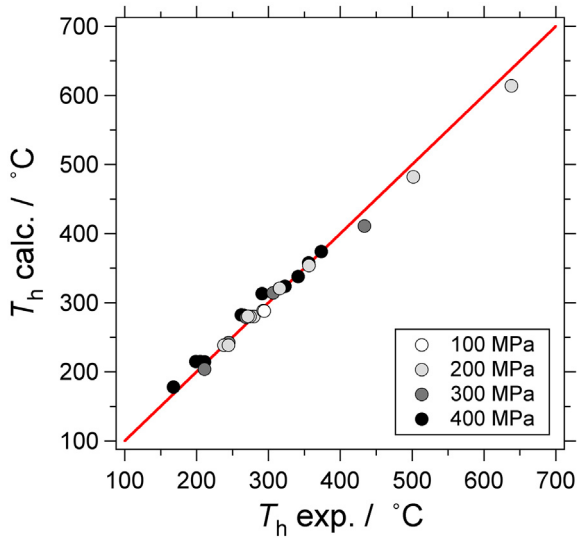

Fig. 7. Correlation between experimental homogenization temperatures (Bodnar, 1994) and calculated homogenization temperatures according to the software AqSo_NaCl (Bakker, 2018).

according to the expansivity and compressibility of the host mineral at a variety of temperature-pressure conditions. The equation of state that describes the variability of the molar volume of quartz (e.g. Hosieni et al., 1985) can be used to calculated modification of the fluid density in fluid inclusions in quartz, as it can be used in the software *AqSo_NaCl* (e.g. Fig. 5a). These modified isochores correspond to iso-T_h lines in fluid inclusion studies, and appear to have highly variable slopes in *p-T* diagrams.

Comparison of a 40 mass% NaCl fluid system between calculation with *AqSo_NaCl* and the model presented by Bodnar (1994, 2003) reveals a variety of differences (Fig. 6). First, iso-T_h curves are significantly curved in the liquid-sold field (i.e. brine and halite) and in the homogeneous liquid field according to *AqSo_NaCl*. Second, iso-T_h curves are not steeper in the liquid-solid field than in the homogeneous liquid field in contrast to the considerations of Bodnar (1994, 2003). Third, the slope of iso-T_h curves in the homogeneous liquid field change significantly at the α-β transition of quartz and may be negative in a small temperature interval close to this transition (see also Fig. 5a). Fourth, the liquidus of 40 mass% NaCl is located at significant higher temperatures. In addition, iso-T_h temperature-pressure values can be directly related to densities with *AqSo_NaCl*, which was not considered in the original model of Bodnar (1994).

Despite these differences between the models, the experimental results from this synthetic fluid inclusion study are consistent with the model presented in *AqSo_NaCl* up to 400 MPa, if you take into account the uncertainties and accuracy of the analyses. The uncertainties of an experimental study are reflected in the spread of homogenization temperatures from a homogeneous synthetic fluid inclusion assemblage. This spread may reach values up to 30˚. The uncertainties are affected by a series of experimental difficulties, including preparation of capsules, experimental loading conditions, temperature-pressure variation during the experiment, unloading *p-T* trajectories (e.g. Bakker, 2017), and accuracy and reproducibility of the analytical method (microthermometry). The average of raw data (T_h and T_m) provided by Bodnar (1994) can be used to calculate average molar volume and composition with *AqSo_NaCl* (Appendix). The obtained composition is slightly lower (39.2 ± 0.2 mass% NaCl) than the experimentally defined value of 40 mass% NaCl. The difference in liquidus temperature (Fig. 6), c.f. 325 °C and 316 °C according to *AqSo_NaCl* and Bodnar (1994), respectively, can be explained by this variation in composition. The corrected composition can be used to calculate homogenization and dissolution temperatures with *AqSo_NaCl* by constructing iso-T_h curves that are defined by the experimental conditions (Appendix). The measured and calculated homogenization temperatures are consistent up to experimental pressures of 400 MPa (Fig. 7). At higher pressures (500 and 600 MPa) calculated homogenization temperatures are up to 50˚ higher than measured values, corresponding to lower densities (Appendix). These discrepancies are explained by the curvature of the iso-T_h curves that are calculated with *AqSo_NaCl*, compared to straight lines of Bodnar (1994, 2003). For example, the 300˚ iso-T_h curve in Fig. 6 is already approximately 100 MPa higher at 600 °C.

Raw microthermometrical data of synthetic fluid inclusions were originally used to design simple purely empirical equations to describe the slope of iso-T_h lines for H_2O-NaCl fluid mixtures up to 40 mass% NaCl (Bodnar, 1994; Bodnar and Vityk, 1994), as a function of salinity and homogenization temperatures. These publications do not provide equations for the conditions of the liquid-vapour envelop (i.e. the bubble-point curve). However, iso-T_h lines cannot be constructed without knowledge of the pressure at homogenization conditions. These conditions were firstly presented by Bodnar (2003), referring to the study of Atkinson (2002) that include purely empirical equations with unknown uncertainties, and an incorrect definition of the *SLV*-curve. Moreover, experimental data were not provided for compositions other than 40 mass% NaCl.

7. Liquidus in fluid inclusion studies

The liquidus of the H_2O-NaCl system can be used to calculate fluid properties in inclusions that homogenize according to *SL* → *L* (e.g. Bodnar, 1994), also known as homogenization by halite disappearance. Becker et al. (2008) and Lecumberri_Sanchez et al. (2012) define a series of relative simple purely empirical equations to calculate the composition, density and pressure of fluid inclusions directly from these dissolution temperatures and corresponding homogenization temperatures, i.e. *SLV* → *SL* and *SL* → *L*, similar to the procedure "Microthermometry" in *AqSo_NaCl* (Bakker, 2018).

The method applied by Becker et al. (2008) to design an empirical model by using the information obtained from synthetic fluid inclusions cannot be reproduced according to the inferior incomplete description. It is assumed that their experiments were performed within the halite-liquid field (*SL* field), by loading an unknown amount of NaCl saturated aqueous solution and halite crystals. Subsequently, heterogeneous trapping processes must have resulted in an assemblage of synthetic

fluid inclusions that mainly contain this NaCl saturated aqueous solution. Other studies of heterogeneous trapping illustrate a large variation in fluid properties of individual inclusions if a liquid and vapour phase are involved (e.g. Bodnar et al., 1985). A certain variation is also expected in the experiments of Becker et al. (2008), but the measurement of only a few inclusions per experiment does not allow an interpretation about the properties of the halite liquidus. Experimental temperatures are not revealed by Becker et al. (2008), but should in theory correspond to the dissolution temperature of halite. However, it is very unlikely that the highly variable temperatures given in Becker et al. (2008) correspond to the externally controlled temperatures of the experiments.

The model of Lecumberri_Sanchez et al. (2012) is based on defining an extensive *pVTx* "pseudo" dataset by using the equation of state defined by Driesner and Heinrich (2007) and Driesner (2007). This "pseudo" dataset was used to define new simpler purely empirical equations only based on the input of the homogenization and dissolution temperatures *SLV* → *SL* and *SL* → *L*, respectively. The simplifications of Lecumberri_Sanchez et al. (2012) can only be applied to a small part of this original model, and introduce a certain loss in accuracy.

The equations of Driesner and Heinrich (2007) and Driesner (2007) are also used in the software *AqSo_NaCl*. It is therefore expected that the values calculated with the model of Lecumberri_Sanchez et al. (2012) correspond to values calculated with *AqSo_NaCl*. However, Fig. 8 illustrates significant differences in the interpretation of T_h and T_m values between the two models. It is evident from the 100 and 300 MPa isobars, i.e. pressure at total homogenization by halite disappearance, and the 30 mass% isopleth (Fig. 8b) that the model of Lecumberri_Sanchez et al. (2012) cannot be extrapolated to temperatures below 100 °C. Significant discrepancies are observed at higher salinities and higher temperatures: the liquidus of the 70 mass% NaCl isopleth at 100 MPa correspond to the microthermometrical data set of 516.6 °C (*SLV* → *SL*) and 575.2 °C (*SL* → *L*) according to *AqSo_NaCl* (Fig. 8c), whereas the model of Lecumberri_Sanchez et al. (2012) results in 548.3 °C and 582.5 °C, respectively. Fig. 8c also illustrates that the volumetric properties of the quartz host modifies significantly the position of the 100 MPa isobar. The resulting homogenization and dissolution temperatures of the example of 70 mass% NaCl are 505.7 °C and 575.2 °C, respectively. Consequently, the discrepancy between the models increases even further if the compressibility of quartz is taken into account, as it can be calculated with *AqSo_NaCl*.

The constant-slope isochores according to Lecumberri_Sanchez et al. (2012) for fluid inclusions that homogenize by halite disappearance are extremely deviating from the model used in *AqSo_NaCl* (see Fig. 6 and Table 1). Deviations up to 180 MPa overpressure are calculated from the 500 °C iso-T_h curve, and down to 90 MPa underpressure for the 200 °C iso-T_h curve. It must be concluded that these so-called correlation equations designed specially for fluid inclusion research are not

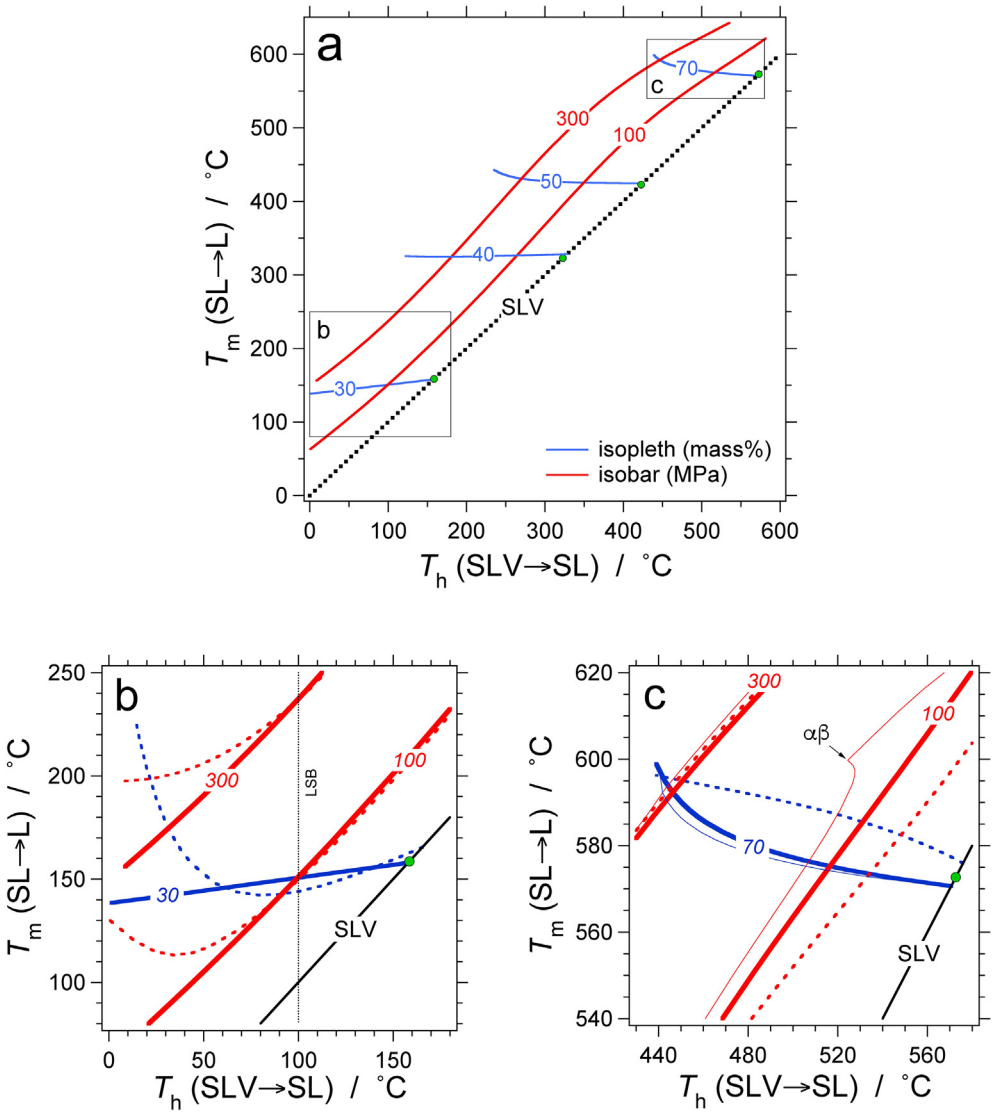

Fig. 8. (**a**) Homogenization temperature (*SLV* → *SL*) versus dissolution temperature (*SL* → *L*) diagram for fluid inclusions with isobars (red lines, numbers in MPa) and isopleths (blue lines, numbers in mass% NaCl). *SLV* is the three phase coexistence curve (halite, brine and vapour). The outlined areas (**b**) and (**c**) are enlarged to elucidate differences between the *AqSo_NaCl* software (thick solid lines) and Lecumberri_Sanchez et al. (2012) (dashed lines). Corrected isobars and isopleths according to the expansivity and compressibility of the host quartz are illustrated with thin lines. *αβ* is the transition of α-quartz to β-quartz. *LSB* is the lower temperature limit (100 °C) of the model according to Lecumberri_Sanchez et al. (2012). The green symbols at the *SLV* curve are values calculated with Bodnar (2003). (For interpretation of the references to colour in this figure legend, the reader is referred to the web version of this article.)

Table 1
Three examples of calculated iso-T_h lines according to Lecumberri_Sanchez et al. (2012) and the software *AqSo_NaCl* (Bakker, 2018). The lines are defined for a 40 mass% NaCl and 70 mass% NaCl fluid system. Dissolution temperatures of halite are not included in the calculations. The iso-T_h lines according to *AqSo_NaCl* are isochores corrected for the modifications of the quartz volume. P_b is the pressure calculated with AqSo_NaCl, P_{LSB} is calculated with Lecumberri_Sanchez et al. (2012).

T_h = 200 °C (*SLV* → *SL*) 40 mass% NaCl			T_h = 300 °C (*SLV* → *SL*) 40 mass% NaCl			T_h = 500 °C (*SLV* → *SL*) 70 mass% NaCl		
T (°C)	P_B (MPa)	P_{LSB} (MPa)	*T* (°C)	P_B (MPa)	P_{LSB} (MPa)	*T* (°C)	P_B (MPa)	P_{LSB} (MPa)
350	316.2	321.6	400	158.3	176.1	600	126.8	198.1
400	476.8	456.3	500	340.7	345.7	650	182.9	328.6
450	679.9	591.0	600	569.5	533.3	700	278.8	459.1

consistent with "comprehensive models" (equations of state) that are not specifically designed to interpret fluid inclusion data. The program *AqSo_NaCl* is offering this consistency.

8. Isobaric and isochoric bubble-point curves

Numerous studies on fluid inclusions present microthermometrical data in a T_m-T_h diagram or a T_h-salinity diagram (e.g. Wilkinson, 2001), which may contain isobaric and isochoric bubble-point curves between the critical curve and the *SLV* curve (e.g. Fig. 9). These curves are often classified as vapour saturated NaCl-H_2O solutions, and refer to dissolution temperatures (*SLV* → *LV*) and homogenization temperatures (*LV* → *L*). The software *AqSo_NaCl* has been used to calculate a number of isobars (10, 50, and 100 MPa) for comparison with those calculated with *HokieFlincs_H2O-NaCl* (Steele-MacInnis et al., 2012) based on the model from Bodnar (2003) (Fig. 9). Substantial differences between the modelled bubble point curves occur already at pressures exceeding 10 MPa. Homogenization temperatures (*LV* → *L*) of the latter may exceed the values from *AqSo_NaCl* up to 200°, whereas salinities may be underestimated by 20 mass%. The most extreme discrepancies occur at higher T_m values (*SLV* → *LV*) corresponding to higher salinities.

Isochores as illustrated in Figs. 1, 3, 4 and 5 do not correspond to isochores that can be constructed in T_m-T_h and T_h-salinity diagrams with bubble-point curves. The former are constructed at constant bulk compositions (isopleth), whereas the bubble-point curves in Fig. 9 are designed for a variety of compositions. Isochoric processes are defined as processes at a constant total volume therefore isochores refer to conditions at constant volume. In a closed system such as fluid inclusions, isochores correspond to conditions of constant density and constant molar volume (e.g. Roedder, 1984; Shepherd et al., 1985; Diamond, 2003b). However, curves of constant density and constant molar volume at bubble point curves do not coincide in T_m-T_h and T_h-salinity diagrams, due to the absence of isopletic conditions. For example, Table 2 illustrates an isochore of constant densities (0.7124 g/cm^3) at variable salinities along the bubble-point curve. A molar volume of 25.29 cm^3/mol is calculated in a pure H_2O system, but this value increases with increasing salinity. At x(NaCl) = 0.15, the molar volume has increased to 33.8 cm^3/mol, whereas the density is still 0.7124 g/cm^3.

Table 2
Properties of the constant-density curve (isochore) of 0.7124 g/cm^3 at bubble-point curves according to the software *AqSo_NaCl* (Bakker, 2018).

x(NaCl)	mass% NaCl	Temperature °C	Pressure MPa	V_m cm^3/mol
0	0	300	8.584	25.2874
0.01	3.1729	320.11	11.119	25.8548
0.02	6.2096	339.79	14.066	26.4224
0.03	9.1185	359.43	17.450	26.9899
0.04	11.9076	379.27	21.222	27.5577
0.05	14.5842	400.2	25.853	28.1251
0.10	26.4954	557.6	75.6757	30.9624
0.15	36.4067	865.8	175.710	33.8001

9. Comparison experimental data and equations

Experimental data of low salinity homogeneous H_2O-NaCl fluid mixtures from Gehrig (1980) is compared to a variety of correlation equations (Zhang and Frantz, 1987; Bodnar, 2003), equations of state (Bowers and Helgeson, 1983; Anderko and Pitzer, 1993), and the program *AqSo_NaCl* (Bakker, 2018).

The modified Redlich-Kwong equation of state (Bowers and Helgeson, 1983) gives accurate numbers in a very limited range of *p-T-V-x* values: at temperatures above 450 °C (Fig. 10a) and pressures below 200 MPa (Fig. 10c and e) up to salinities of 20 mass% NaCl. High density values, i.e. low molar volumes are only poorly reproduced by this equation (Fig. 10b, d, and f). The modified Lee-Kesler equation of state (Anderko and Pitzer, 1993) give accurate numbers for *p-T-V-x*

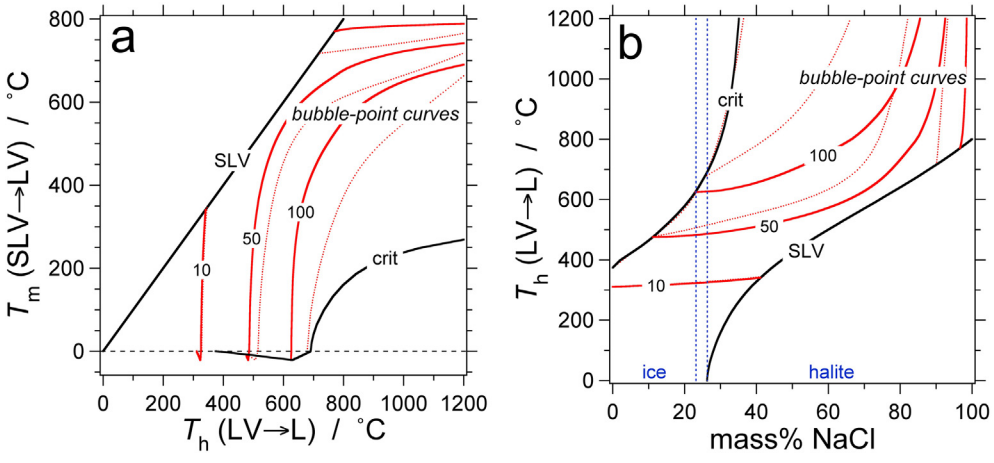

Fig. 9. T_m-T_h diagram (**a**) and T_h-salinity diagram (**b**) with the isobars 10, 50, and 100 MPa at bubble point curves according to *AqSo_NaCl* (solid red curves) and according to *HokieFlincs_H2O-NaCl* (dashed red lines). The critical curve and *SLV* curve are obtained from *AqSo_NaCl* (black lines). Dissolution temperatures at the critical curve in (**a**) reveal values < 0 °C at compositions below the peritectic point (T_h < 698.7 °C). The boundaries between ice, hydrohalite and halite dissolution are illustrated with vertical blue dashed lines in (**b**). (For interpretation of the references to colour in this figure legend, the reader is referred to the web version of this article.)

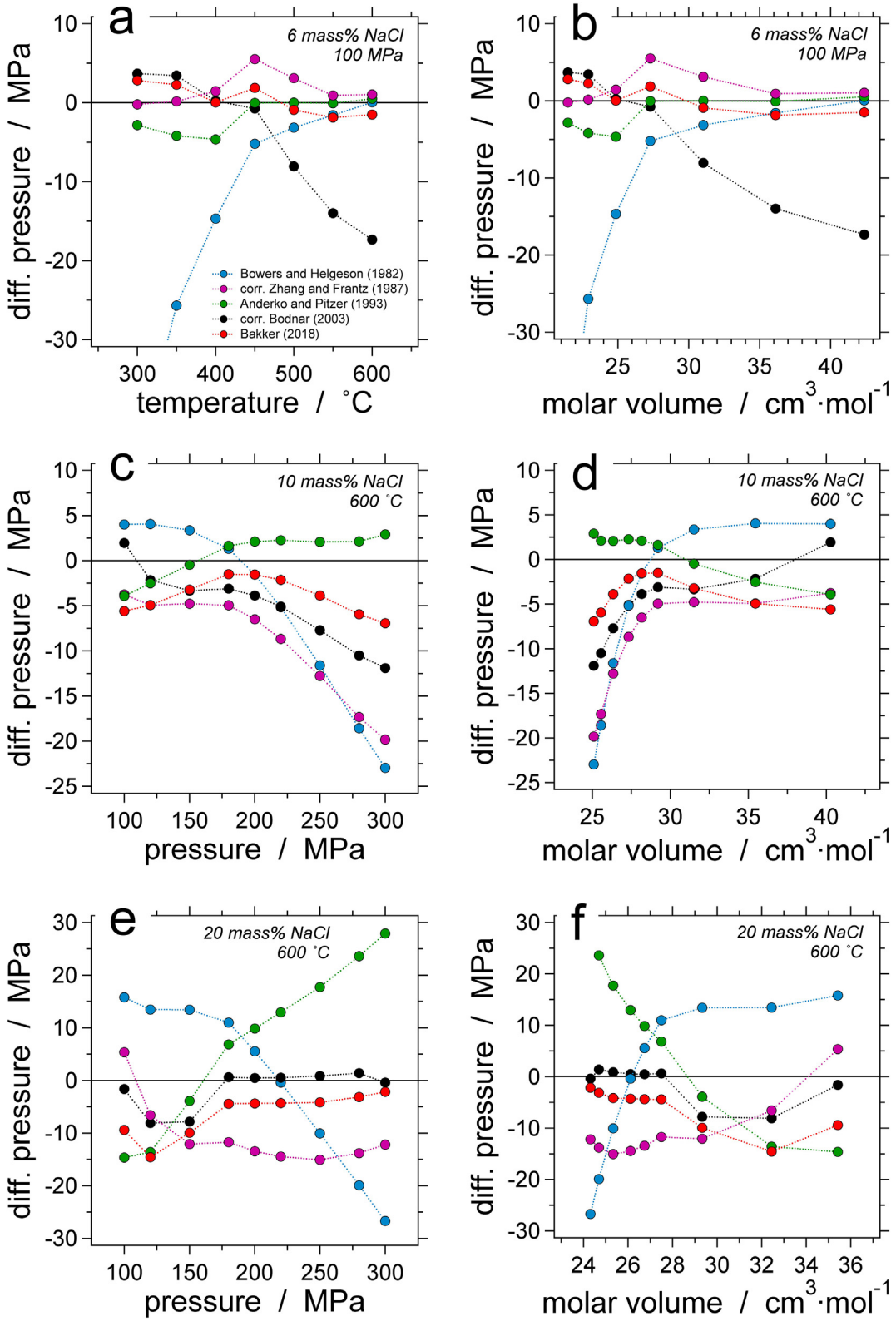

Fig. 10. Pressure difference calculations of a homogeneous H_2O-NaCl fluid mixture between experimental data from Gehrig (1980) and a series of equations at a variety of temperatures, pressures and molar volumes. Examples at bulk salinities of 6 mass% (**a** and **b**), 10 mass% (**c** and **d**) and 20 mass% (**e** and **f**) are illustrated. See text for further details.

parameters up to 10 mass% NaCl (Fig. 10a, b, c, d), whereas the accuracy becomes less at higher salinities (Fig. 10e and f). This equation of state cannot be used below 300 °C, due to mathematical restrictions.

The correlation equations defined by Zhang and Frantz (1987) have similar accuracies as those of Bodnar (2003) at 10 and 20 mass% NaCl (Fig. 10c, d, e, and f). At 6 mass% NaCl, Zhang and Frantz (1987) provide excellent equations, whereas Bodnar (2003) loses accuracy at higher temperatures (Fig. 10a and b). At 600 °C, both correlation

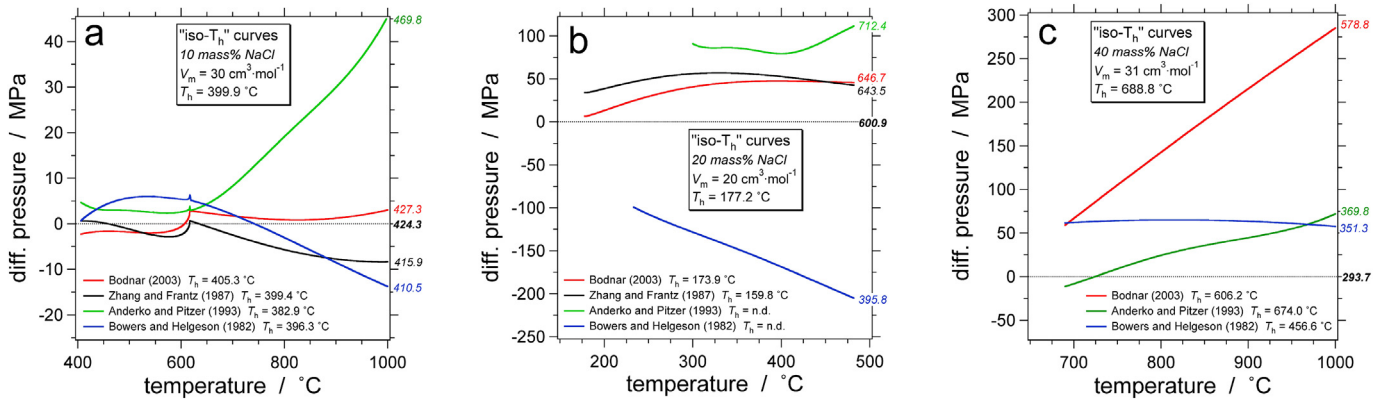

Fig. 11. Pressure difference calculations of *iso-T_h* curves between the *AqSo_NaCl* model (Bakker, 2018) and a series of correlation equations and equations of state. The molar volume and T_h values calculated with *AqSo_NaCl* are illustrated in the shaded boxes in (**a**) for 10 mass% NaCl, in (**b**) for 20 mass% NaCl, and in (**c**) for 40 mass% NaCl. The calculated absolute pressures (in MPa) at 1000 °C of all equations are illustrated at the right-hand side of the diagrams. The bold black values are the pressures calculated with *AqSo_NaCl*. The kinks in the curves in (**a**) correspond to the α-β quartz transition. See text for further detail.

equations are increasingly in error at higher pressures (Fig. 10c and d), similar to deviations of the Bowers and Helgeson equation of state. Zhang and Frantz (1987) cannot be used for salinities exceeding 21 mass% NaCl.

Conditions where you can use these equations have to be investigated in detail to be able to produce accurate numbers, and the application is always restricted to a very limit composition, density, temperature and pressure range. These detailed analyses can be omitted by using *AqSo_NaCl* because it gives the best average accuracy for all conditions illustrated in Fig. 10. Further details about the uncertainties and accuracy can be found in Driesner (2007).

The same correlation equations and equations of state are used to compare iso-T_h lines with the results from *AqSo_NaCl* (Fig. 11). At relative low salinities (< 10 mass%) the 400 °C iso-T_h line is calculated for a molar volume of 30 cm^3/mol. According to the same molar volume, iso-T_h lines calculated with the other equations are similar up to 650 °C (Fig. 11a). However, these equations result in slightly different T_h values, varying between 382.9 and 405.3 °C. At higher temperatures, the Anderko and Pitzer (1993) equation is increasingly deviating from the *AqSo_NaCl* model, up to a difference of 45 MPa at 1000 °C, whereas the other equations remain close to the values calculated with *AqSo_NaCl*. At 20 mass% NaCl, the equations of state (Anderko and Pitzer, 1993; and Bowers and Helgeson, 1983) are highly different along the entire temperature range, and homogenization conditions cannot be calculated (Fig. 11b). The correlation equations (Zhang and Frantz, 1987; Bodnar, 2003) are similar to *AqSo_NaCl*, and result in about 45 MPa overpressure at 500 °C. At 40 mass % NaCl, the opposite effect is observed: the correlation equation of Bodnar (2003) is extremely deviating, whereas the equations of state (Anderko and Pitzer, 1993; and Bowers and Helgeson, 1983) remain within about 60 MPa overpressure (Fig. 11c). The correlation equation of Zhang and Frantz (1987) cannot be used at these high salinities.

10. Conclusions

The software *AqSo_NaCl* (Bakker, 2018) offers a large pallet of calculation procedures to determine the properties of binary H_2O-NaCl systems in fluid inclusions and pore systems. The calculations represent the most accurate mathematical model to characterize the *p-T-V-x* properties in the complete compositional range between pure H_2O and pure NaCl, at temperatures up to 1000 °C and pressures up to 500 MPa. The software can be downloaded from the website of Ronald J. Bakker at the Montanuniversity of Leoben (*http://fluids.unileoben.ac.at*) and from the supplementary data related to the publication in Computer and Geosciences (https://doi.org/10.1016/j.cageo.2018.03.003).

Acknowledgement

This research did not receive any specific grant from funding agencies in the public, commercial, or not-for-profit sectors. I would like to thank Alfons van den Kerkhof for devoting time to reviewing this manuscript.

Supplementary data

Supplementary data to this article can be found online at https://doi.org/10.1016/j.chemgeo.2019.07.041.

Appendix

Comparison experimental data (Bodnar, 1994) and calculations with the software AqSo_NaCl (Bakker, 2018).
Order of changes in phase assemblages within fluid inclusions during a heating experiment: SLV → SL → L.

Bodnar (1994)				*AqSo_NaCl* (Bakker, 2018)				
Exp. cond.		Microthermometry		Calculated from microthermometry		Calculated from experimental conditions		
T_f °C	P_f MPa	T_h (°C) (SLV → SL)	T_m (°C) (SL → L)	V_m cm^3·mol^{-1}	Mass% NaCl	V_f cm^3·mol^{-1}	T_h (°C) (SLV → SL)	T_m (°C) (SL → L)
350	100	292.7	319	22.1693	39.2953	22.0957	288.26	318.86
350	100	294	320.7	22.1967	39.4354	22.0982	288.05	320.51
350	200	238	315.5	21.2984	39.1557	21.2934	238.71	315.53
350	200	244.2	315.3	21.3895	39.1231	21.2922	238.73	315.13

400	200	279.4	318	21.9475	39.2490	21.9540	280.04	318.03
400	200	274.1	317.9	21.8633	39.2552	21.9542	280.04	318.10
400	200	271.5	313.6	21.8052	38.9074	21.9441	280.31	313.92
450	200	315.2	323.6	22.5657	39.6237	22.6819	320.91	323.81
450	200	315.7	322.7	22.5713	39.5444	22.6803	321.00	322.90
350	300	211.1	310.1	20.8981	38.7936	20.7622	204.08	309.88
400	300	244.6	313.8	21.3900	39.0001	21.3277	242.43	313.73
450	300	269.3	316.2	21.7792	39.1278	21.9261	279.02	316.54
500	300	306.6	321.8	22.4126	39.4936	22.5695	314.38	322.07
350	400	167.7	311.9	20.3517	39.0225	20.4100	178.19	312.14
400	400	205.2	312.9	20.8287	39.0276	20.9039	215.09	313.20
400	400	210.9	305.9	20.8802	38.4669	20.8716	214.58	306.04
400	400	199	313.6	20.7492	39.0960	20.9079	215.15	314.06
500	400	265.6	312.1	21.7065	38.8021	21.9593	282.09	312.70
500	400	262.2	316.7	21.6693	39.1890	21.9779	282.26	317.39
550	400	291.1	320.3	22.1472	39.4096	22.5579	313.37	321.06
600	400	323.1	323.7	22.6817	39.6074	23.1586	323.97	338.85
400	500	156.5	312.7	20.2240	39.0972	20.5919	194.03	313.49
400	500	157	315.8	20.2412	39.3249	20.6077	194.44	316.42
500	500	236.5	314.4	21.2724	39.0705	21.5501	258.25	315.13
500	500	216.7	316.5	20.9985	39.2880	21.5636	258.53	317.78
500	500	222.3	317.6	21.0807	39.3641	21.5683	258.63	318.70
600	500	281.6	321.4	21.9950	39.5290	22.6046	314.89	322.50
400	600	153.4	315.9	20.2004	39.3347	20.3617	177.62	316.22
400	600	144.7	312.5	20.0908	39.0953	20.3429	176.99	313.07
500	600	191.5	313.2	20.6504	39.0800	21.2223	239.18	314.61
600	600	246	316.9	21.4222	39.2491	22.1647	292.72	318.46
600	600	245.3	313.9	21.4009	39.0063	22.1487	292.32	315.54
600	600	240.6	314.6	21.3335	39.0758	22.1532	292.44	316.38
700	600	293.4	321.7	22.1902	39.5221	23.1524	322.87	332.55
700	600	290.9	319.8	22.1422	39.3679	23.1435	321.03	332.01

Comparison experimental data (Bodnar, 1994) and calculations with the software AqSo_NaCl (Bakker, 2018).
Order of changes in phase assemblages within fluid inclusions during a heating experiment: SLV → LV → L.

Bodnar (1994)				*AqSo_NaCl* (Bakker, 2018)				
Exp. cond.		Microthermometry		Calculated from microthermometry		Calculated from experimental conditions		
T_f °C	P_f MPa	T_h (°C) (LV → L)	T_m (°C) (SLV → LV)	V_m $cm^3 \cdot mol^{-1}$	Mass% NaCl	V_f $cm^3 \cdot mol^{-1}$	T_h (°C) (LV → L)	T_m (°C) (SLV → LV)
500	200	356.3	325	23.4235	39.6704	23.4671	353.92	324.97
700	200	501.7	327.7	27.0678	39.6566	27.3763	482.32	327.34
800	200	638.3	328.9	29.4152	39.5950	29.8331	613.81	328.55
700	300	433.4	323.6	25.3932	39.4266	25.4790	411.22	323.15
600	400	341.4	319.9	23.0912	39.2614	23.1463	337.98	319.85
650	400	356	324	23.4177	39.5858	23.7734	357.85	324.04
700	400	373.6	323.1	23.7873	39.4865	24.4087	373.98	323.11
700	500	327.7	323.9	22.7958	39.6169	23.6947	346.98	324.22
700	500	336.1	327.8	22.9726	39.9407	23.7084	347.92	328.01
700	500	329.2	326.9	22.8270	39.8725	23.7055	347.72	327.21

References

Anderko, A., Pitzer, K.S., 1993. Equation-of-state representation of phase equilibria and volumetric properties of the system NaCl-H_2O above 573 K. Geochim. Cosmochim. Acta 57, 1657–1680.

Atkinson, A.B., 2002. A Model for the PTX Properties of H_2O-NaCl. Unpublished M.S. Thesis. Virginia Tech, Blacksburg VA (133 pp.).

Bakker, R.J., 2012. Can the vapour phase be neglected to estimate bulk salinity of halite bearing aqueous fluid inclusions. Cent. Eur. J. Geosci. 4, 238–245.

Bakker, R.J., 2017. Re-equilibration processes in fluid inclusion assemblages. Minerals 7, 117. https://doi.org/10.3390/min7070117.

Bakker, R.J., 2018. AqSo_NaCl: computer program to calculate p-T-V-x properties in the H_2O-NaCl fluid system applied to fluid inclusion research and pore fluid calculation. Comput. Geosci. 115, 122–133.

Bakker, R.J., Diamond, L.W., 2006. Estimation of volume fractions of liquids and vapor phases in fluid inclusions, and definition of inclusion shapes. Am. Mineral. 91, 635–657.

Becker, S.P., Fall, A., Bodnar, R.J., 2008. Synthetic fluid inclusions: XVII. PVTX properties of high salinity H_2O-NaCl solutions (> 30 wt% NaCl): application to fluid inclusions that homogenize by halite disappearance from porphyry copper and other hydrothermal ore deposits. Econ. Geol. 103, 539–554.

Bodnar, R.J., 1994. Synthetic fluid inclusions. XII. Experimental determination of the liquidus and isochores for a 40 wt% H_2O-NaCl solution. Geochim. Cosmochim. Acta 58, 1053–1063.

Bodnar, R.J., 1995. Experimental determination of the PVTX properties of aqueous solutions at elevated temperatures and pressures using synthetic fluid inclusions: H_2O-NaCl as an example. Pure Appl. Chem. 67, 873–880.

Bodnar, R.J., 2003. Introduction to aqueous-electrolyte fluid inclusions. In: Samson, I., Anderson, A., Marshall, D. (Eds.), Fluid Inclusions: Analysis and Interpretation. 32. Mineral. Assoc. Can. Short Course Ser, pp. 81–100.

Bodnar, R.J., Vityk, M.O., 1994. Interpretation of microthermometric data for H_2O-NaCl fluid inclusions. In: De Vivo, B., Frezzotti, M.L. (Eds.), Fluid Inclusions in Minerals: Methods and Applications. Virginia Tech, Blacksburg VA, pp. 117–130.

Bodnar, R.J., Burnham, C.W., Sterner, S.M., 1985. Synthetic fluid inclusions in natural quartz. III. Determination of phase equilibrium properties in the system H_2O-NaCl to 1000 °C and 1500 bars. Geochim. Cosmochim. Acta 49, 1861–1873.

Bowers, T.S., Helgeson, H.C., 1983. Calculation of the thermodynamic and geochemical consequences of non-ideal mixing in the system H_2O-CO_2-NaCl on phase relations in geological systems: equation of state for H_2O-CO_2-NaCl fluids at high pressures and temperatures. Geochim. Cosmochim. Acta 47, 1247–1275.

Bucher, K., Grapes, R., 2010. Petrogenesis of Metamorphic Rocks, eight ed. Springer-Verlag, Heidelberg.

Diamond, L.W., 2003a. Systematics of H_2O inclusions. In: Samson, I., Anderson, A., Marshall, D. (Eds.), Fluid Inclusions: Analysis and Interpretation. Mineral. Assoc. Can. Short Course Ser 32. pp. 55–79.

Diamond, L.W., 2003b. Glossary: Terms and symbols used in fluid inclusion studies. In: Samson, I., Anderson, A., Marshall, D. (Eds.), Fluid Inclusions: Analysis and Interpretation. Mineral. Assoc. Can. Short Course Ser. 32. pp. 365–374.
Driesner, T., 2007. The system H_2O-NaCl. Part II: Correlations for molar volume, enthalpy, and isobaric heat capacity from 0 to 1000 °C, 1 to 5000 bar, and 0 to 1 X_{NaCl}. Geochim. Cosmochim. Acta 71, 4902–4919.
Driesner, T., Heinrich, C.A., 2007. The system H_2O-NaCl. Part I. Correlation formulae for phase relations in temperature-pressure-composition space from 0 to 1000 °C, 0 to 5000 bar, and 0 to 1 X_{NaCl}. Geochim. Cosmochim. Acta 71, 4880–4901.
Duan, Z., Li, D., 2008. Coupled phase and aqueous species equilibrium of the H_2O-CO_2-NaCl-$CaCO_3$ system from 0 to 250 °C, 1 to 1000 bar with NaCl concentrations up to saturation of halite. Geochim. Cosmochim. Acta 72, 5128–5145.
Gehrig, M., 1980. Phasengleichgewichte und pVT-Daten ternärer Mischungen aus Wasser, Kohlendioxid und Natriumchlorid bis 3 kbar und 550 °C. Diss. ret. nat. Karlsruhe, HochschulVerlag, Freiburg.
Gehrig, M., Lentz, H., Franck, E.U., 1986. The system water carbon-dioxide sodium-chloride to 773 K and 300 MPa. Ber. Bunsengesell. 90, 525–533.
Haar, L., Gallagher, J.S., Kell, G.S., 1984. NBS/NRC Steam Tables. Hemisphere Publishing Corporation, Washington.
Holdaway, M.J., Mukhopadhyay, B., 1993. A re-evaluation of the stability relations of andalusite: thermodynamical data and phase diagram for the aluminium silicates. Am. Mineral. 78, 298–315.
Hosieni, K.R., Howald, R.A., Scanlon, M.W., 1985. Thermodynamics of the lambda transition and the equation of state of quartz. Am. Mineral. 70, 782–793.
Lecumberri_Sanchez, P., Steele-MacInnis, M., Bodnar, R.J., 2012. A numerical model to estimate trapping conditions of fluid inclusions that homogenize by halite disappearance. Geochim. Cosmochim. Acta 92, 14–22.
Leisen, M., Dubessy, J., Boiron, M.-C., Lach, P., 2012. Improvement of the determination of element concentrations in quartz-hosted fluid inclusions by LA-ICP-MS and Pitzer thermodynamic modelling of ice melting temperature. Geochim. Cosmochim. Acta 90, 110–125.
Newton, R.C., Manning, C.E., 2000. Quartz solubility in H_2O-NaCl and H_2O-CO_2 solutions at deep crust-upper mantle pressures and temperatures: 2-15 kbar and 500-900 °C. Geochim. Cosmochim. Acta 64, 2993–3005.
Pettke, T., Oberli, F., Audetat, A., Guillong, M., Simon, A.C., Hanley, J.J., Klemm, L.M., 2012. Recent developments in element concentration and isotope ratio analysis of individual fluid inclusions by laser ablation single and multiple collector ICP-MS. Ore Geol. Rev. 44, 10–38.
Roedder, E., 1984. Fluid Inclusions, Reviews in Mineralogy 12. Mineralogical Society of America, Washington DC.
Shepherd, T.J., Rankin, A.H., Alderton, D.H.M., 1985. A Practical Guide to Fluid Inclusion Studies. Blackie, Glasgow and London.
Span, R., Wagner, W., 1996. A new equation of state for carbon dioxide covering the fluid region from the triple point temperature to 1100 K at pressures up to 800 MPa. J. Phys. Chem. Ref. Data 25, 1509–1596.
Steele-MacInnis, M., Lecumberri-Sanchez, P., Bodnar, R.J., 2012. HokieFlincs_H2O-NaCl: a microsoft Excel spreadsheet for interpreting microthermometric data from fluid inclusions based on the PVTX properties of H_2O-NaCl. Comput. Geosci. 48, 334–337.
Sterner, S.M., Hall, D.L., Bodnar, R.J., 1988. Synthetic fluid inclusions. V. Solubility relations in the system NaCl-KCl-H_2O under vapor-saturated conditions. Geochim. Cosmochim. Acta 52, 989–1006.
Wilkinson, J.J., 2001. Fluid inclusions in hydrothermal ore deposits. Lithos 55, 229–272.
Winter, J.D., 2014. Principles of Igneous and Metamorphic Petrology, eight ed. Pearson new International Edition, Harlow.
Zhang, Y.-G., Frantz, J.D., 1987. Determinations of the homogenization temperatures and densities of supercritical fluids in the system NaCl-KCl-$CaCl_2$-H_2O using synthetic fluid inclusions. Chem. Geol. 64, 335–350.